Plasma Processes and Polymers

PLASMA PROCESSES AND POLYMERS

RESEARCH ARTICLE OPEN ACCESS

Complex Stimuli Induced by Surface Discharge Method Enable Minimally Invasive and High-Efficiency Macromolecule Delivery Into *Chlamydomonas reinhardtii*

Kazuki Tange | Taiki Hirohata | Yoshihisa Ikeda | Masafumi Jinno

Department of Electrical and Electronic Engineering, Ehime University, Matsuyama, Japan

Correspondence: Kazuki Tange (tange.kazuki.nz@ehime-u.ac.jp)

Received: 30 October 2025 | **Revised:** 3 April 2026 | **Accepted:** 4 May 2026

Funding: Society for the Promotion of Science (JSPS) in the form of KAKENHI, Grant/Award Numbers: 25H02215, 24H02250, 24H02536, 23H01165, 21H04265; Ehime University Research Unit Program

Keywords: *Chlamydomonas reinhardtii* | endocytosis | macromolecule delivery | surface discharge

ABSTRACT

Intracellular delivery of macromolecules into microalgae has been constrained by rigid cell walls. This study presents a high-efficiency, high-viability method for delivering macromolecules into *Chlamydomonas reinhardtii* using surface discharge plasma. At a nominal voltage of 25 kV, which produced a favorable balance between delivery efficiency and cell viability, the method achieved > 40% efficiency for 250 kDa FITC-dextran while maintaining > 80% viability. Under the same conditions, 2 MDa FITC-dextran was also delivered. Orthogonal cross-sectional analysis confirmed intracellular cargo localization. Delivery results from cellular responses to plasma-induced complex stimuli; the ~60% reduction highlights endocytosis as a major pathway, whereas the remaining fraction may involve multifaceted processes such as transient membrane permeabilization. This integrated approach enables minimally invasive macromolecule entry into microalgae.

1 | Introduction

Microalgae are promising biological resources because of their rapid growth and high photosynthetic efficiency. They accumulate diverse nutraceuticals, pharmaceuticals, and lipids that serve as feedstocks for biofuels, making them attractive for use across industries such as food, medicine, and energy [1–4]. However, to realize these applications commercially, it is essential to improve intrinsic biological characteristics, or "traits," of the algae themselves, such as enhancing lipid productivity for biodiesel and ensuring stable production of valuable compounds for food and pharmaceutical use. Accordingly, developing efficient intracellular delivery systems for functional molecules is a prerequisite essential to realize these biotechnological advancements [5, 6]. In this study, we used the unicellular green alga *Chlamydomonas reinhardtii* as a model organism. *Chlamydomonas* is a key model system across diverse biological fields, including photosynthesis, ciliary dynamics, and cell cycle regulation. It offers major advantages through its well-annotated genome and suitability for genetic manipulation [7].

Despite this, technologies for intracellular delivery of foreign molecules, fundamental to trait enhancement, remain underdeveloped [8]. The main obstacle is the presence of a rigid, distinctive cell wall composed of a complex lattice of hydroxyproline-rich glycoproteins (HRGPs) [9]. Conventional physical and biological methods each present serious drawbacks, as summarized in Table 1. Moreover, most previous studies have assessed delivery efficiency based on the number of stable transformants obtained after DNA introduction. Reports

Abbreviations: FITC, fluorescein isothiocyanate; MβCD, methyl-β-cyclodextrin; TAP, tris-acetate-phosphate.

This is an open access article under the terms of the Creative Commons Attribution License, which permits use, distribution and reproduction in any medium, provided the original work is properly cited.

© 2026 The Author(s). Plasma Processes and Polymers published by Wiley-VCH GmbH.

TABLE 1 | Comparison of macromolecule delivery methods for *Chlamydomonas reinhardtii*.

Method	Delivered molecule	Target cell line	Delivery efficiency (%)	Cell viability (%)	Key features & challenge
Glass bead[10]	Plasmid DNA	Wall-deficient	Not comparable[a]	Low-to-moderate[b]	**Features**: Simple, inexpensive; no special equipment or consumables required. **Challenges**: Inapplicable to wild-type cells with cell walls; low efficiency.
Electroporation[11, 12]	BSA (~67 kDa)	Wild-type	~2	~50 (PI Staining[c])	**Features**: Highly versatile for small molecule delivery. **Challenges**: Very inefficient for macromolecule delivery into wild-type cells; requires specialized equipment and consumables (i.e., cuvettes); exhibits significant efficiency-viability trade-off.
	BSA (~67 kDa)	Wall-deficient	~10	~20 (PI Staining[c])	
	FITC-dextran (40 kDa)	Wild-type	Not comparable[a]	~30 (Photosynthetic Quantum Yield[d])	
Particle gun[13]	DNA, RNP	Wild-type	Not comparable[a]	Moderate[e]	**Features**: Only method capable of organelle delivery (i.e., mitochondria). **Challenges**: Very low efficiency; requires specialized equipment and consumables (i.e., gold/tungsten particles); carries a risk of DNA damage.
Cell-penetrating peptides[14]	BSA (~67 kDa)	Wild-type	~25–80	~45-7 (Colony-forming ability[f])	**Features**: No special equipment required; high delivery efficiency. **Challenges**: Severe cytotoxicity; high running costs associated with reagents (i.e., peptides).
	Alcohol dehydrogenase (150 kDa)	Wild-type	~26	< 45 (Colony-forming ability[f])	
Electromechanical poration[15]	FITC-Dextran (2 MDa)	Wild-type	~30	~65 (FDA staining[g])	**Features**: Achieves both high efficiency and high viability for very large molecule delivery. **Challenges**: Low throughput makes it unsuitable for large-scale processing; it requires specialized equipment and complex operation.
Surface discharge (this study)	FITC-dextran (250 kDa)	Wild-type	41.3	82.6	**Features**: Mitigates efficiency-viability trade-offs associated with conventional methods. Enables macromolecule delivery with high efficiency and very high viability. No specialized consumables are required. General-purpose dishes can also be used, resulting in low running costs. This method is scalable and suitable for large-scale processing. **Challenges**: Requires specialized equipment.
	FITC-dextran (2 MDa)	Wild-type	5.8	87.4	

[a]Efficiency is evaluated by transformant numbers or relative fluorescence levels. This makes direct comparison with the initial uptake rate (%) difficult.
[b]A viability level of 25% was reported after 60 s of agitation, but specific data regarding the optimal agitation time (10–20 s) remains unknown.
[c]PI Staining: Assesses immediate membrane damage.
[d]Photosynthetic Quantum Yield: Assesses metabolic health.
[e]Many studies focus on obtaining transformants, and comparable quantitative viability data remains limited.
[f]Colony-forming ability: A stringent metric assessing long-term reproductive capacity.
[g]FDA Staining: Assesses enzymatic activity within live cells.

directly evaluating the initial physical delivery rate across the total cell population are rare, likely because this rate is extremely low with existing approaches and has thus been considered impractical for comparison. Based on limited comparable data, electroporation clearly shows severe limitations for macromolecule delivery. When macromolecules such as BSA (~ 67 kDa) are introduced, delivery efficiency reaches an upper limit of only about 2%, and severe cytotoxicity accompanies these conditions, reducing cell viability to approximately 50% [11]. Even recently developed advanced techniques continue to face similar challenges, particularly in balancing efficiency with viability. For example, the cell-penetrating peptide method faces a similar cytotoxicity issue: increasing delivery efficiency from 25% to over 80% sharply decreases viability, as measured by colony-forming ability, from 45% to 7% [14]. Likewise, while electromechanical poration, which combines electrical stimuli with mechanical stress to enhance permeability, achieves excellent local performance using a single microinjector, it cannot be scaled efficiently for large populations of cells [15]. Thus, existing methods face an inherent trade-off between efficiency and viability, and no scalable, minimally invasive macromolecule delivery technique has yet been established.

To address these challenges, we focused on atmospheric-pressure plasma technology. This approach has been investigated in numerous life-science applications, including wound healing, cancer therapy, and stimulation of seed germination and yield improvement [16–20]. Specifically, recent studies in plasma medicine have shown that the integrated effects of electric fields and chemical factors, including reactive oxygen and nitrogen species (RONS), enhance cell membrane permeability across diverse systems. These advances span applications ranging from antibacterial treatments using air plasma devices [21, 22] to integrated approaches, such as combining plasma-treated solutions with electroporation [23] and developing plasma aerosol protocols for large-surface delivery [24]. In this context, direct plasma exposure has also been applied to the delivery of functional molecules, including genes and drugs. Examples include the introduction of Cas9 ribonucleoprotein (RNP) complexes [25], delivery mediated by intracellular Ca^{2+} signaling [26], and DNA delivery via plasma-activated air [27].

We have previously shown that combined electrical and chemical stimuli generated from microplasma induce endocytosis—an intrinsic cellular uptake process—enabling minimally invasive gene delivery [28–35]. This finding established a new mechanistic framework for plasma-induced molecular internalization. The interdependent roles of RONS and electric fields, including the relative contributions of endocytic pathways, have also been extensively evaluated in other contexts, such as cancer cell treatment [36, 37]. Moreover, electrical equivalent circuit modeling has revealed that current flow through the cell membrane is a key factor influencing delivery efficiency [29]. Nevertheless, the microplasma technique we developed has a major limitation: it requires cells to adhere to the bottom of a well during treatment, making it unsuitable for large-scale processing of continuously suspended cells such as *Chlamydomonas*.

To overcome this technical constraint, we employed a "surface discharge method," which is better suited for large-scale processing of suspended cells. Like the microplasma approach, it applies electrochemical stimuli to cell suspensions and operates on the same basic principles while being scalable to large populations.

Our previous work demonstrated that, in animal cells, approximately 80% of the surface discharge-mediated delivery proceeds via endocytosis [30]. However, it has remained entirely unclear how these relative contributions change in microalgae with rigid cell walls, or how the wall itself affects the delivery process. Therefore, the present study first evaluates whether the surface discharge method enables efficient macromolecule delivery into *Chlamydomonas* by (1) quantifying delivery efficiency and cell viability for model macromolecules of different molecular weights (250 kDa and 2 MDa), and (2) investigating the delivery mechanism by examining the multifaceted contributions of endocytosis and other potential uptake processes in the presence of a robust microalgal cell wall.

2 | Experimental Section

2.1 | Algal Culture and Sample Preparation

The wild-type strain of *Chlamydomonas reinhardtii* (CC-124, NIES-2238) was provided by the National Institute for Environmental Studies (NIES) through the National BioResource Project (NBRP) of the Ministry of Education, Culture, Sports, Science and Technology (MEXT), Japan. The cell was cultured in 100 mL of Tris-Acetate-Phosphate (TAP) medium at 25°C under continuous illumination (82 μmol photons m^{-2} s^{-1}) with shaking at 100 rpm. During the exponential growth phase, cells (1×10^6 to 6×10^6 cells mL^{-1}) were counted using a hemocytometer and centrifuged at 600× *g* for 5 min. The resulting pellet was resuspended in 10% TAP medium to a final concentration of 1×10^8 cells mL^{-1}. For molecular uptake experiments, two sizes of FITC-dextran (Sigma; 250 kDa and 2 MDa) were used at final concentrations of 100 μM and 10 μM, respectively. Since these molecules emit green fluorescence, their uptake could be observed and quantified using a fluorescence microscope.

2.2 | Surface Discharge Method

Figure 1 shows the schematic diagram and electrode configuration of the surface discharge apparatus used for molecular delivery. Four stainless steel needle electrodes (diameter: 0.7 mm) were employed: two connected to the power source and two to ground. A 3.5 cm dish was first filled with 1 mL of 1% albumin solution, which was aspirated and removed, followed by 1 mL of sterile water that was also aspirated. Albumin pretreatment improved dish wettability, allowing the cell suspension to spread evenly. Subsequently, 100 μL of the cell suspension was added, and a 20 kHz sine wave was applied to the electrodes. Discharge was performed at preset voltages of 20, 25, and 30 kV to evaluate voltage dependence, while the discharge duration was fixed at 20 ms. The relationship between these nominal settings and the corresponding measured peak-to-peak voltages (V_{p-p}) is described in Section 3.1. This duration was selected as the standard condition based on preliminary trials in which it provided a balanced compromise between inducing molecular uptake and maintaining cell viability. The gap

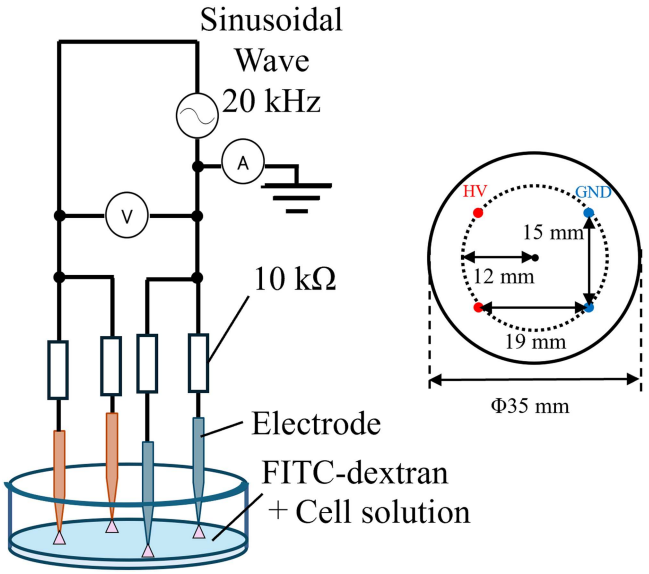


FIGURE 1 | Schematic of the configuration used for molecular delivery by the surface discharge method. V and A indicate the measurement points for actual applied voltage and discharge current, respectively.

between the electrode tip and the suspension surface was maintained at 1 mm. To characterize the discharge, waveforms were monitored using a digital oscilloscope (4 Series MSO, Tektronix). Signals were recorded in normal acquisition mode with a sampling interval of 0.8 ns (1.25 GS/s) to enable high-resolution detection of transient events. After treatment, 3 mL of TAP medium was added, and cells were collected into a 5 mL tube. Following one wash, 2 mL of TAP medium and 2 mL of 0.2% trypan blue were added, and the mixture was incubated at 25°C for 10 min. The cells were then washed again and finally resuspended in TAP medium.

2.3 | Analysis of Viable Cells and Fluorescence

Samples were examined using a fluorescence microscope (BZ-X810), and the number of cells exhibiting FITC-dextran uptake was determined. The condition without surface discharge served as the control. A cell was classified as "fluorescent" when its fluorescence intensity exceeded the background level observed in 99% of untreated control cells. Delivery efficiency was calculated as the ratio of fluorescent cells to total cells. For orthogonal cross-sectional analysis, Z-stack images were acquired using an LSM7DUO confocal laser scanning microscope (Carl Zeiss) equipped with an EC Plan-Neofluar 40×/1.30 Oil DIC M27 objective lens. Excitation was performed at 489 nm for FITC and chlorophyll autofluorescence. Emission signals were collected within wavelength ranges of 500–550 nm for FITC and 650–710 nm for chlorophyll. Z-stack images were captured with a step size of 0.44 μm. Orthogonal cross-sectional views (XZ and YZ planes) were reconstructed using ImageJ to assess the intracellular localization of the delivered macromolecules. Cell viability was assessed using trypan blue staining, and the percentage of *Chlamydomonas* cells excluding trypan blue was recorded as the viable fraction.

2.4 | Investigation of Cellular Uptake Mechanism Using Inhibitors

To elucidate the uptake mechanism, prior to adding FITC-dextran, the TAP medium was replaced with medium containing the endocytosis inhibitor methyl-β-cyclodextrin (MβCD), and cells were incubated for 1 h at 25°C. The final MβCD concentration was 30 mM. After incubation, the inhibitor was removed by centrifugation, and the cells were washed twice with 10% TAP medium. The treated cells were then subjected to the surface discharge procedure described above. FITC-dextran-positive and viable cells were subsequently counted to determine delivery efficiency and viability.

3 | Results

3.1 | Electrical and Visual Characteristics of Surface Discharge and Its Effect on Delivery Performance

To characterize the physical stimuli applied to cells, the electrical properties of the four-pin electrode system were analyzed. As expected, both peak discharge current and total energy delivered increased with applied voltage (Figure 2). The actual measured peak-to-peak voltages (V_{p-p}) during discharge were 12.0, 15.1, and 17.7 kV, corresponding to nominal settings of 20, 25, and 30 kV, respectively. At the nominal 20, 25, and 30 kV conditions (V_{p-p} = 12.0, 15.1, and 17.7 kV), the peak discharge current reached 28.7, 42.6, and 66.0 mA, respectively. Power dissipation across the 10 kΩ series resistors was estimated to be 5–8% of the total peak power over the measured voltage range. Since this ohmic loss was less than 10%, it was considered negligible, and the calculated energy density (19.5 J/mL at 25 kV) was used for subsequent evaluations. Similarly, energy densities at 20 and 30 kV were determined to be 10.2 and 36.1 J/mL, respectively.

Detailed waveform analysis revealed distinct asymmetry in ignition patterns between the positive and negative voltage phases (Figure 2, inset). During the positive half-cycle, discharge ignition typically appears as a steep, step-like current rise that stabilizes at a higher level. In contrast, the negative half-cycle is characterized by clusters (bursts) of multiple impulsive spikes. In both phases, each individual event exhibits a rapid leading edge with a rise time of less than 50 ns. These rapid transient events, featuring high dI/dt, together with the sustained current magnitude, provide the primary physical stimuli likely affecting multiple cellular uptake pathways, as discussed in Section 4.

Visual observation confirmed the operational mode and stability of the discharge. Figure 3a shows the electrode setup under ambient light, whereas Figure 3b illustrates plasma emission in the dark. The plasma ignited independently at each of the four electrode tips and made direct contact with the liquid surface rather than bridging the electrodes through the gas phase, characterizing the system as a plasma-assisted electrochemical process. As the nominal applied voltage increased from 20 to 30 kV, the discharge area visibly expanded and luminosity intensified, while stable, localized footprints on the liquid surface were maintained. Electrically, increasing voltage resulted

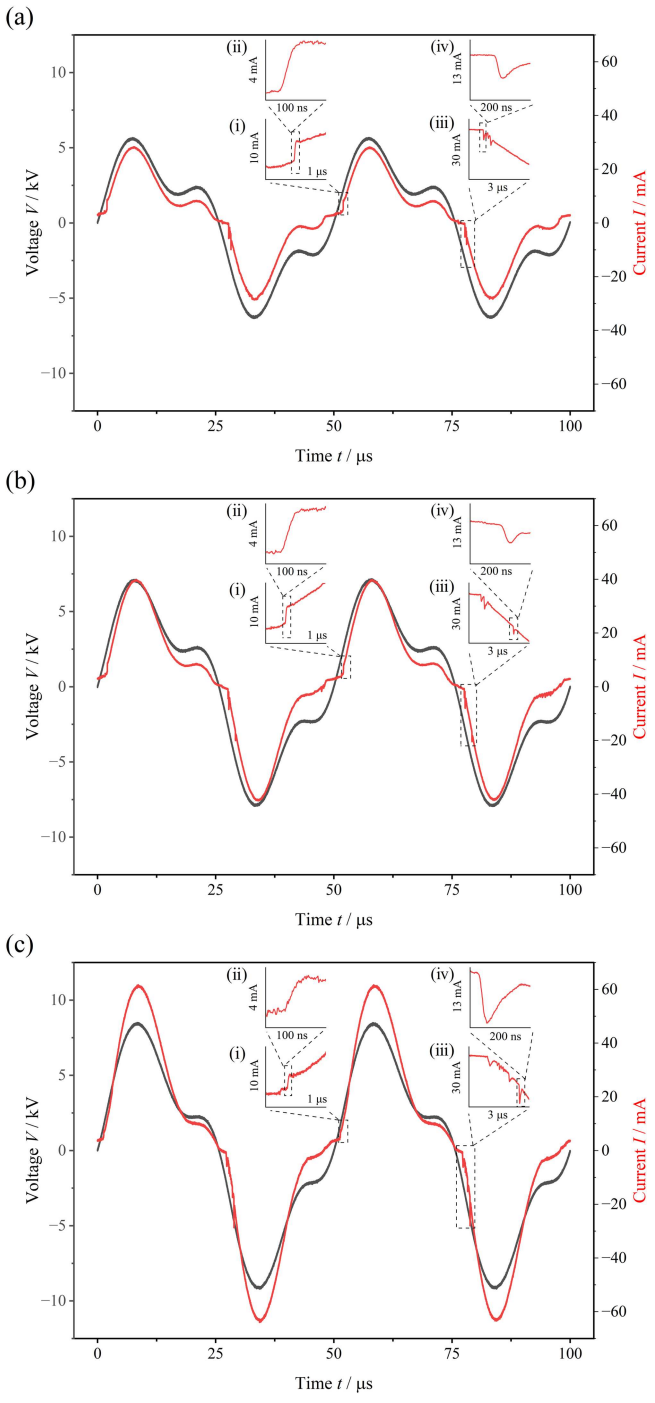


FIGURE 2 | Comparative analysis of discharge waveforms at applied voltages of 20, 25, and 30 kV. (a) 20 kV, (b) 25 kV (optimized condition), and (c) 30 kV. Each panel shows the overall voltage (black) and current (red) waveforms. The four insets provide a hierarchical and symmetrical view of the discharge characteristics: (i, iii) the discharge activity during the positive and negative phases, respectively, shown on an identical microsecond scale to contrast the discrete discharge events in the positive phase with the intermittent pulse trains in the negative phase; (ii, iv) nanosecond-scale profiles of representative single pulses from each phase, highlighting the steep rising edges used for evaluation of dI/dt. All corresponding plots across (a–c) are kept at identical scales to facilitate direct comparison of discharge intensities and temporal behaviors.

in a higher baseline current amplitude; however, the characteristic filamentary peaks remained consistent across all conditions, indicating that the fundamental discharge regime was maintained throughout the tested voltage range.

The biological effects of the applied stimuli were evaluated by measuring the delivery efficiency of 250 kDa FITC-dextran and cell viability across different voltages (Figure 4). Fluorescence microscopy confirmed successful delivery into *Chlamydomonas reinhardtii* under all conditions (Figure 4a). Delivery efficiencies were 17.5%, 41.3%, and 36.9% at 20, 25, and 30 kV, respectively (Figure 4c), while the corresponding cell viabilities were 87.1%, 82.6%, and 73.6%, indicating a decline with increasing energy input (Figure 4b). These findings indicate that the nominal voltage of 25 kV provides a favorable balance between delivery efficiency and cell survival in this experimental system.

To confirm that the macromolecules were internalized rather than merely adsorbed onto the cell surface, orthogonal cross-sectional analysis was performed using confocal microscopy. As shown in Figure 4d, three-dimensional localization of the green fluorescence confirmed that 250 kDa FITC-dextran was clearly situated within the cell interior, specifically enclosed by the red-fluorescing chloroplast.

3.2 | Delivery of Large Molecules (2 MDa)

Since delivery mechanisms may vary depending on molecular size, we next attempted to deliver a larger molecule. FITC-dextran of 2 MDa (2000 kDa) was introduced at an applied voltage of 25 kV. Fluorescence microscopy verified that 2 MDa FITC-dextran was successfully taken up by Chlamydomonas cells (Figure 5a). Increasing molecular size from 250 kDa to 2 MDa did not noticeably affect cell viability (Figure 5b). However, the delivery efficiency markedly decreased from 41.3% to 5.8%. However, delivery efficiency decreased sharply from 41.3% to 5.8% (Figure 5c). Furthermore, to assess the degree of intracellular accumulation, the mean fluorescence intensity (MFI) was quantified on 10 randomly selected fluorescence-positive cells from each group. The results showed that MFI per cell declined significantly from 10.9 ± 2.3 a.u. for the 250 kDa condition to 8.4 ± 0.8 a.u. for the 2 MDa condition (Student's t-test, $p < 0.01$). These findings indicate that a larger molecular size markedly reduces both the probability of cellular uptake and the degree of intracellular accumulation.

3.3 | Investigation of Delivery Mechanism Using an Endocytosis Inhibitor

To assess the role of endocytosis in molecular delivery by surface discharge, we performed experiments using the inhibitor methyl-β-cyclodextrin (MβCD). Preliminary tests confirmed that *Chlamydomonas* cells showed no cytotoxicity at 30 mM MβCD (Figure 6a). This concentration is higher than the 10 mM level known to cause toxicity in human dermal fibroblasts, as previously reported [30]. Consequently, subsequent inhibitor

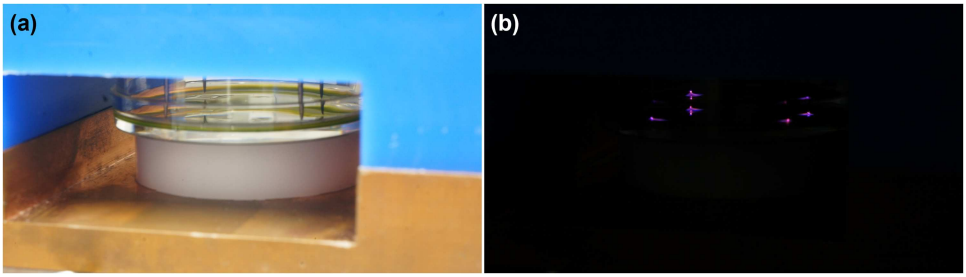


FIGURE 3 | Visual observation of the surface discharge setup and operation. (a) Electrode configuration above the cell suspension under ambient light. (b) Plasma emission captured in the dark at an applied voltage of 25 kV (V_{p-p}). The plasma ignites independently at the tips of the four needle electrodes and directly contacts the liquid surface. Secondary light points observed near the rear electrodes represent optical reflections from the liquid–dish interface, not additional discharge sites.

treatments were carried out at this 30 mM [30]. Cells pretreated with MβCD were then subjected to delivery of 250 kDa FITC-dextran under standard conditions (25 kV, 20 ms). MβCD treatment reduced delivery efficiency by approximately 60% (relative efficiency: 0.4), though a significant 40% portion of the delivery was retained (Figure 6b).

4 | Discussion

In this study, we demonstrated that the surface discharge method effectively delivers macromolecules into the microalga *Chlamydomonas*, despite its rigid cell wall. The observed increase in delivery efficiency as the applied voltage was raised from 20 kV to 25 kV likely reflects both the greater current passing through the cells and the enhanced generation of RONS, consistent with the measured rise in total input energy density. Although precise quantification of RONS during the brief 20 ms discharge is challenging due to rapid reaction kinetics, their production is generally proportional to the total energy input. However, at 30 kV, excessive current and RONS appear to cause lethal cellular damage, thereby reducing delivery efficiency. These findings indicate that precise control of stimulus intensity enables this method to achieve both high delivery efficiency and high viability.

To evaluate the invasiveness of this approach, it is instructive to compare these results with conventional electroporation (EP) protocols. According to Azencott et al. [11], EP wild-type Chlamydomonas exhibits a severe trade-off between delivery efficiency and cell viability. In their study, as energy levels increased, macromolecule delivery efficiency remained approximately 2%, while the cell mortality rate rose steadily. At a membrane potential of 1.2 V (corresponding to a calculated energy of 26.1 J/mL), the survival rate dropped to approximately 1%, with no improvement in delivery efficiency. In contrast, the surface discharge method achieved a delivery efficiency of approximately 40% with 82.6% viability at 25 kV (19.5 J/mL). Even at the highest energy level of 36.1 J/mL (30 kV), cell viability remained above 70%.

The simultaneous achievement of high viability and high delivery efficiency suggests that the input energy is not expended solely as a uniform, lethal electric-field stress. Instead, the energy appears to be effectively partitioned into multiple stimuli, including biochemical signals (RONS) and localized nanosecond-scale physical triggers. Specifically, electrical stimulation—comprising a continuous current component and high dI/dt transient events—acts as a part of the complex stimuli alongside RONS-induced chemical stress to activate multiple delivery pathways. Our previous study on animal cells showed that intracellular currents, coupled with RONS, serve as a direct driving force for endocytosis [31]. Our results suggest that these plasma-induced complex stimuli induce active endocytosis in microalgae, while the combination of high dI/dt transient events and continuous current may also cause transient changes in membrane permeability. By distributing total energy across multiple moderate stimulation modes, the system prevents any single stress factor from exceeding the lethal threshold and is thought to effectively function as a "switch" that reconfigures membrane permeability while maintaining structural integrity.

The successful delivery of a 250 kDa molecule with over 40% efficiency is particularly significant. This result suggests the potential to deliver cargoes comparable in size to the Cas9 RNP complexes (approximately 250 kDa) used in CRISPR/Cas9 genome editing. The orthogonal views (Figure 4d) provide clear visual confirmation of successful intracellular delivery, reinforcing the reliability of the surface discharge method for introducing large, functional cargo into walled microalgal cells. We also achieved the delivery of a 2 MDa macromolecule comparable in size to a typical plasmid vector (approximately 2−3 MDa). The cell wall of *C. reinhardtii* represents a primary physical barrier to macromolecule entry. Plasma treatment is thought to modulate wall structure to facilitate delivery. For instance, Ikeda et al. [38] reported that plasma treatment induces morphological changes in land plant cells through localized decomposition of structural components, including the cuticular and pectin layers. These changes are attributed to the integrated action of chemically active species—particularly ·OH radicals, which cleave polysaccharide chains—alongside Joule heating generated by the discharge current. We propose that similar biochemical and thermal reconfiguration of the microalgal cell wall enhances the accessibility of large cargo to the plasma membrane. However, increasing the molecular size from 250 kDa to 2 MDa markedly reduced delivery efficiency, likely due to the greater physical resistance encountered when traversing both the cell wall and plasma membrane, even with plasma-induced wall modifications. Nevertheless, the ability to deliver plasmid-sized molecules while maintaining high viability demonstrates the method's potential for introducing gene expression cassettes.

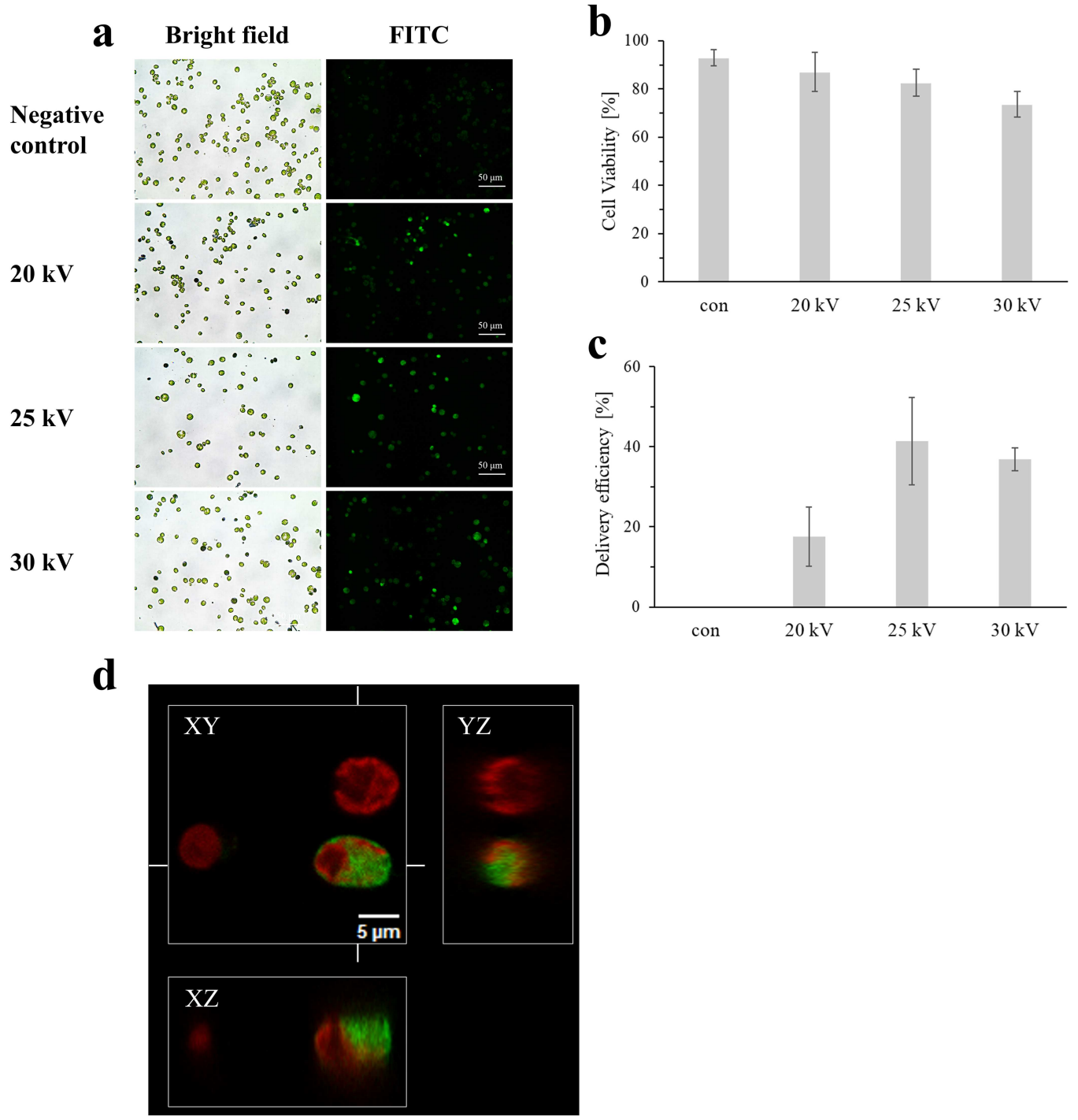


FIGURE 4 | (a) Fluorescence microscopy images showing the delivery of 250 kDa FITC–dextran into wild-type *Chlamydomonas reinhardtii* using the surface discharge method at different applied voltages. The discharge duration was 20 ms, and the final FITC-dextran concentration was 100 µM. Following treatment, cells were washed, stained with trypan blue, and imaged. The negative control group was exposed to FITC–dextran without surface discharge treatment. (b) Cell viability at each applied voltage. (c) Delivery efficiency of FITC–dextran at different applied voltages. (d) Orthogonal views (XY, XZ, and YZ planes) of a *Chlamydomonas* cell after surface discharge at 25 kV, confirming intracellular localization of 250 kDa FITC–dextran. The green fluorescence signal is fully confined within the cup-shaped chloroplast (red autofluorescence). White markers at the image borders indicate the slice positions for the corresponding cross-sections. Scale bar: 5 µm.

Regarding the delivery mechanism, the 60% reduction in efficiency following MβCD treatment indicates that endocytosis is a major delivery pathway in microalgae, consistent with our previous findings in animal and plant cells [31, 38, 39]. MβCD is known to disrupt lipid rafts by depleting cholesterol from the plasma membrane, thereby inhibiting clathrin-mediated endocytosis [40]. Our results confirm that this MβCD-sensitive route represents a principal delivery mechanism in Chlamydomonas. Recent evidence shows that the Arp2/3 complex is essential for endocytosis in *Chlamydomonas*, with endocytic activity and associated actin structures increasing markedly upon cellular stimulation [41]. Furthermore, exposure to cold

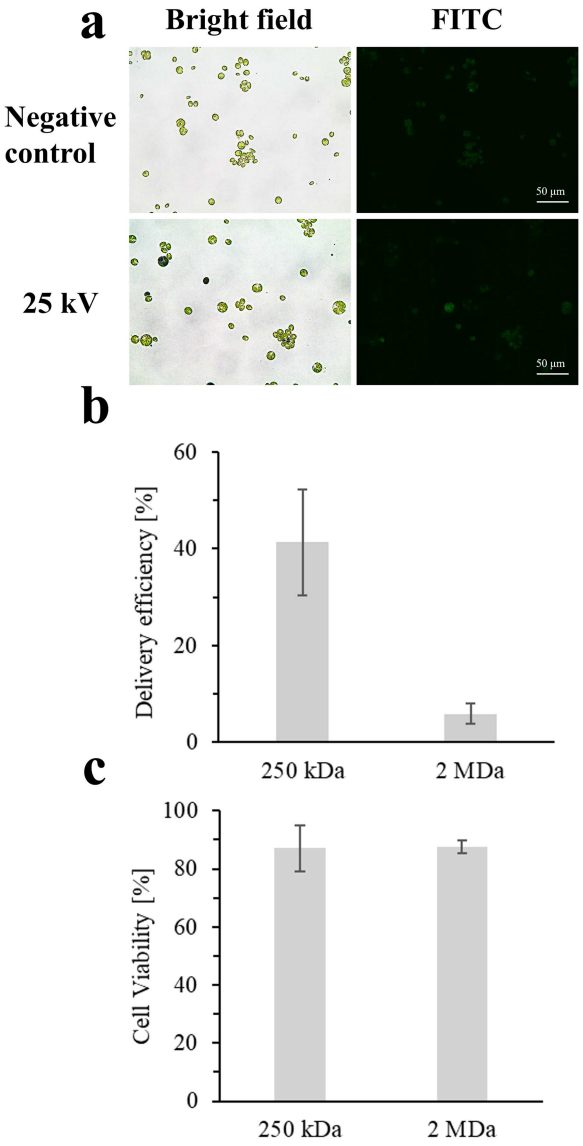


FIGURE 5 | (a) Fluorescence microscopy images showing the delivery of 2 MDa FITC–dextran into *Chlamydomonas reinhardtii* using the surface discharge method. (b) Cell viability corresponding to different FITC–dextran molecular sizes. (c) Delivery efficiency of FITC–dextran molecules of various sizes into cells.

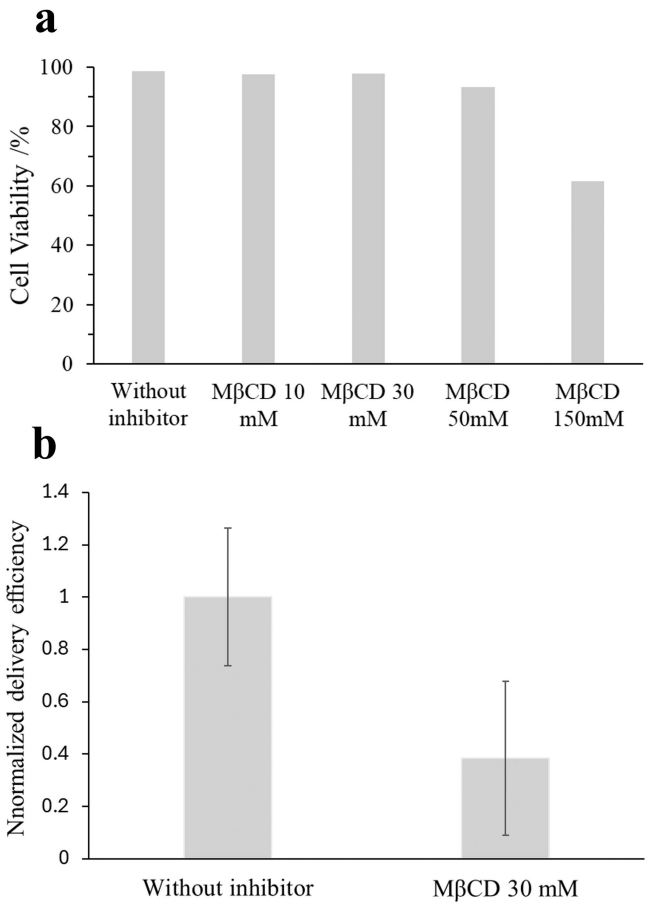


FIGURE 6 | (a) Cell viability of *Chlamydomonas reinhardtii* treated with different concentrations of methyl-β-cyclodextrin (MβCD). (b) Normalized delivery efficiency of 250 kDa FITC–dextran in *Chlamydomonas* cells pretreated with MβCD. The final inhibitor concentration was 30 mM. After 1 h of incubation, MβCD was removed by centrifugation, and cells were subsequently exposed to surface discharge at an applied voltage of 25 kV.

atmospheric plasma has been shown to induce Arp2/3-dependent structural changes and sustained cellular responses [42]. Given that the Arp2/3 complex orchestrates cellular responses to environmental forces, it is plausible that the physical and chemical stressors generated during surface discharge activate this intrinsic mechanosensitive machinery, thereby contributing to the observed macromolecule uptake [43]. The involvement of reactive species as chemical stimuli in this process aligns with findings in other plasma systems [28, 44]. Although these studies employed different plasma sources and biological targets, RONS consistently emerge as critical triggers for macromolecule delivery. For example, the ROS scavenger NAC markedly inhibits delivery [28], and uptake efficiency depends on gas-derived species, such as hydroxyl (·OH) radicals [44]. In our system, RONS are considered essential stimuli for activating the signaling networks that mediate endocytosis.

Conversely, the ~40% delivery efficiency retained after MβCD treatment suggests that the delivery mechanism does not rely on a single pathway. This residual efficiency may reflect incomplete inhibition of endocytosis by the inhibitor or the presence of endocytic pathways insensitive to MβCD. Furthermore, electrical stimulation—comprising high dI/dt transient events and continuous current—could potentially contribute to transient changes in membrane permeability, such as localized physical pore formation. Molecular dynamics simulations of electroporation provide a theoretical basis for such transient pore formation under sustained electrical stress [45]. This supports our interpretation that the integrated action of these electrical components provides the necessary physical impulse and sustained force for membrane permeabilization. Therefore, the mechanism of this method is proposed as an integrated combination of multiple physical and biological processes driven by plasma-derived complex stimuli, likely providing a basis for the delivery efficiency observed even in microalgae with robust cell walls.

Regarding the practical application of this method, it is important to recognize that different microalgal species may respond variably to plasma treatment. Variations in cell wall

robustness and physiological sensitivity mean that the optimal plasma "dose"—defined as the combination of treatment duration and applied voltage—must be adjusted for each target strain. Careful adjustment of these parameters to accommodate specific physiological characteristics is essential to achieve comparable delivery efficiency while maintaining high viability. Future studies should focus on identifying the underlying signaling networks and determining the optimal plasma dose for each microalgal species.

5 | Conclusion

In this study, we demonstrated the delivery of high-molecular-weight markers (250 kDa and 2 MDa FITC-dextran) into the model microalga *Chlamydomonas reinhardtii* using the surface discharge method. At a nominal applied voltage of 25 kV, a delivery efficiency of 41.3% was achieved while maintaining a high cell viability of 82.6%.

The favorable performance of this method is attributed to the integrated action of complex electrical and chemical stimuli associated with surface discharge. Several factors likely contribute in an integrated manner: (1) transient structural modulation of the cell wall induced by discharge stress, (2) activation of cellular uptake processes through the combined stimuli of discharge current and RONS, and (3) transient membrane permeability changes involving high dI/dt transients and steady current.

Mechanistic analysis using the inhibitor MβCD suggested that approximately 60% of the delivery is mediated by endocytosis, with the remaining delivery potentially involving multifaceted processes, including endocytic pathways insensitive to the inhibitor or transient physical membrane permeabilization. This integrated model aligns with recent biological insights into endocytosis and simulation results on physical membrane permeabilization.

Overall, these results demonstrate that the surface discharge method provides a minimally invasive and highly efficient approach for the delivery of macromolecules into microalgae with rigid cell walls. Its simplicity and high efficiency highlight its potential as a fundamental platform for delivering functional molecules (such as RNPs and plasmids) in future genetic engineering applications. Verifying the biological functional expression of molecules introduced using this approach is a key future objective.

Author Contributions

Kazuki Tange was involved in conceptualization, investigation, writing – original draft, and project management. Taiki Hirohata was involved in review and editing. Masafumi Jinno and Yoshihisa Ikeda were involved in conceptualization, writing – review, and editing.

Acknowledgments

The authors would like to thank the National BioResource Project (NBRP), Japan, for providing the *Chlamydomonas reinhardtii* strain (NIES-2238). This study was partly supported by Japan Society for the Promotion of Science (JSPS) in the form of KAKENHI grants (25H02215, 24H02250, 24H02536, 23H01165, 21H04265) and the Ehime University Research Unit Program.

Conflicts of Interest

The authors declare no conflicts of interest.

Data Availability Statement

The data that support the findings of this study are available from the corresponding author upon reasonable request.

References

1. T. M. Mata, A. A. Martins, and N. S. Caetano, "Microalgae for Biodiesel Production and Other Applications: A Review," *Renewable and Sustainable Energy Reviews* 14 (2010): 217–232.

2. M. Olaizola, "Commercial Development of Microalgal Biotechnology: From the Test Tube to the Marketplace," *Biomolecular Engineering* 20, no. 4–6 (2003): 459–466, https://doi.org/10.1016/S1389-0344(03)00076-5.

3. G. Huang, F. Chen, D. Wei, X. Zhang, and G. Chen, "Biodiesel Production by Microalgal Biotechnology," *Applied Energy* 87 (2010): 38–46.

4. M. J. Griffiths and S. T. L. Harrison, "Lipid Productivity as a Key Characteristic for Choosing Algal Species for Biodiesel Production," *Journal of Applied Phycology* 21 (2009): 493–507.

5. R. Radakovits, R. E. Jinkerson, A. Darzins, and M. C. Posewitz, "Genetic Engineering of Algae for Enhanced Biofuel Production," *Eukaryotic Cell* 9 (2010): 486–501.

6. M. Fayyaz, K. W. Chew, P. L. Show, T. C. Ling, I.-S. Ng, and J.-S. Chang, "Genetic Engineering of Microalgae for Enhanced Biorefinery Capabilities," *Biotechnology Advances* 43 (2020): 107554.

7. S. Sasso, H. Stibor, M. Mittag, and A. R. Grossman, "The Natural History of Model Organisms: From Molecular Manipulation of Domesticated *Chlamydomonas reinhardtii* to Survival in Nature," *eLife* 7 (2018): e39233, https://doi.org/10.7554/eLife.39233.

8. M. F. Ortiz-Matamoros, M. A. Villanueva, and T. Islas-Flores, "Genetic Transformation of Cell-Walled Plant and Algae Cells: Delivering DNA Through the Cell Wall," *Briefings in Functional Genomics* 17 (2018): 26–33.

9. E. Cronmiller, D. Toor, N. C. Shao, T. Kariyawasam, M. H. Wang, and J.-H. Lee, "Cell Wall Integrity Signaling Regulates Cell Wall-Related Gene Expression in *Chlamydomonas reinhardtii*," *Scientific Reports* 9 (2019): 12204.

10. K. L. Kindle, "High-Frequency Nuclear Transformation of *Chlamydomonas reinhardtii*," *Proceedings of the National Academy of Sciences* 87 (1990): 1228–1232.

11. H. R. Azencott, G. F. Peter, and M. R. Prausnitz, "Influence of the Cell Wall on Intracellular Delivery to Algal Cells by Electroporation and Sonication," *Ultrasound in Medicine & Biology* 33 (2007): 1805–1817.

12. K. Jeon, A. Suresh, and Y. C. Kim, "Highly Efficient Molecular Delivery into *Chlamydomonas reinhardtii* by Electroporation," *Korean Journal of Chemical Engineering* 30 (2013): 1626–1630.

13. Z. Hu, Z. Fan, Z. Zhao, J. Chen, and J. Li, "Stable Expression of Antibiotic-Resistant Gene *ble* from *Streptoalloteichus hindustanus* in the Mitochondria of *Chlamydomonas reinhardtii*," *PLoS One* 7 (2012): e35542, https://doi.org/10.1371/journal.pone.0035542.

14. S. Kang, A. Suresh, and Y.-C. Kim, "A Highly Efficient Cell Penetrating Peptide pVEC-Mediated Protein Delivery System into Microalgae," *Algal Research* 24 (2017): 360–367.

15. W. Huang, S. Sakuma, N. Tottori, S. S. Sugano, and Y. Yamanishi, "Viscosity-Aided Electromechanical Poration of Cells for Transfecting Molecules," *Lab on a Chip* 22 (2022): 4276–4291.

16. T. Hirata, T. Kishimoto, C. Tsutsui, T. Kanai, and A. Mori, "Healing Burns Using Atmospheric Pressure Plasma Irradiation," *Japanese Journal of Applied Physics* 53 (2014): 010302.

17. H. Tanaka, M. Mizuno, Y. Katsumata, et al., "Oxidative Stress-Dependent and -Independent Death of Glioblastoma Cells Induced by Non-Thermal Plasma-Exposed Solutions," *Scientific Reports* 9 (2019): 13657.

18. H. Sakakita and Y. Ikehara, "Irradiation Experiments on a Mouse Using a Mild-Plasma Generator for Medical Applications," *Plasma and Fusion Research* 5 (2010): S2117.

19. T. Okumura, H. Tanaka, T. Nakao, et al., "Health Assessment of Rice Cultivated and Harvested From Plasma-Irradiated Seeds," *Scientific Reports* 13 (2023): 17450.

20. K. Koga, S. Thapanut, T. Amano, et al., "Simple Method of Improving Harvest by Nonthermal Air Plasma Irradiation of Seeds of *Arabidopsis thaliana* (L.)," *Applied Physics Express* 9 (2016): 016201.

21. Q. Zhang, J. Zhuang, T. von Woedtke, et al., "Synergistic Antibacterial Effects of Treatments With Low Temperature Plasma Jet and Pulsed Electric Fields," *Applied Physics Letters* 105 (2014): 104103, https://doi.org/10.1063/1.4895731.

22. R. Mentheour and Z. Machala, "Coupled Antibacterial Effects of Plasma-Activated Water and Pulsed Electric Field," *Frontiers in Physics* 10 (2022): 895813, https://doi.org/10.3389/fphy.2022.895813.

23. T. H. Chung, A. Stancampiano, K. Sklias, et al., "Cell Electropermeabilisation Enhancement by Non-Thermal-Plasma-Treated PBS," *Cancers* 12 (2020): 219, https://doi.org/10.3390/cancers12010219.

24. V. Vijayarangan, Z. Maaroufi, A. Rouillard, et al., "Plasma Jet and Plasma Treated Aerosol Induced Permeation of Reconstructed Human Epidermis," *Bioelectrochemistry* 167 (2026): 109060, https://doi.org/10.1016/j.bioelechem.2025.109060.

25. Y. Yanagawa, Y. Suenaga, Y. Iijima, et al., "Genome Editing by Introduction of Cas9/sgRNA into Plant Cells Using Temperature-controlled Atmospheric Pressure Plasma," *PLoS One* 18 (2023): e0281767, https://doi.org/10.1371/journal.pone.0281767.

26. S. Sasaki, Y. Hokari, A. Kumada, M. Kanzaki, and T. Kaneko, "Direct Plasma Stimuli Including Electrostimulation and OH Radical Induce Transient Increase in Intracellular Ca2+and Uptake of a Middle-Size Membrane-Impermeable Molecule," *Plasma Processes and Polymers* 15 (2018): 1700077, https://doi.org/10.1002/ppap.201700077.

27. C. M. Edelblute, L. C. Heller, M. A. Malik, and R. Heller, "Activated Air Produced by Shielded Sliding Discharge Plasma Mediates Plasmid DNA Delivery to Mammalian Cells," *Biotechnology and Bioengineering* 112 (2015): 2583–2590.

28. M. Jinno, S. Satoh, Y. Ikeda, and H. Motomura, "The New Technology of Molecular and Gene Introduction Method Using Discharge Plasma: Plasma Brings Features of Random Genome Integration-Free and Damage-Free to Cells, Genomic-DNA and External Introducing Molecules," *Japanese Journal of Applied Physics* 60 (2021): 030502.

29. Y. Kido, H. Motomura, Y. Ikeda, S. Satoh, and M. Jinno, "Clarification of Electrical Current Importance in Plasma Gene Transfection by Equivalent Circuit Analysis," *PLoS One* 16 (2021): e0245654, https://doi.org/10.1371/journal.pone.0245654.

30. T. Hiramatsu, H. Hirashige, Y. Kido, S. Satoh, and M. Jinno, "Importance of Collision Frequency in the Molecular Size Dependency of Gene Transfer Efficiency in the Surface Discharge Method," *Japanese Journal of Applied Physics* 58 (2019): SEEG05.

31. M. Jinno, Y. Ikeda, H. Motomura, Y. Isozaki, Y. Kido, and S. Satoh, "Synergistic Effect of Electrical and Chemical Factors on Endocytosis in Micro-Discharge Plasma Gene Transfection," *Plasma Sources Science and Technology* 26 (2017): 065016.

32. M. Jinno, Y. Ikeda, H. Motomura, Y. Kido, and S. Satoh, "Investigation of Plasma Induced Electrical and Chemical Factors and Their Contribution Processes to Plasma Gene Transfection," *Archives of Biochemistry and Biophysics* 605 (2016): 59–66.

33. K. Ikeda and H. Sumiya, "Optical Properties of Ultrapure Nano-Polycrystalline Diamond," *Japanese Journal of Applied Physics* 55 (2016): 07LG06.

34. M. Jinno, Y. Ikeda, H. Motomura, Y. Kido, K. Tachibana, and S. Satoh, "The Necessity of Radicals for Gene Transfection by Discharge Plasma Irradiation," *Journal of Photopolymer Science and Technology* 27 (2014): 399–404.

35. Y. Isozaki, Y. Ikeda, Y. Kido, S. Satoh, and M. Jinno, "Reactive Oxygen Species and Intracellular Ca2+ Contribution to Micro-Discharge Plasma Gene Transfection," *Plasma Medicine* 7 (2017): 321–332.

36. V. Vijayarangan, A. Delalande, S. Dozias, J.-M. Pouvesle, C. Pichon, and E. Robert, "Cold Atmospheric Plasma Parameters Investigation for Efficient Drug Delivery in HeLa Cells," *IEEE Transactions on Radiation and Plasma Medical Sciences* 2 (2018): 109–115.

37. V. Vijayarangan, A. Delalande, S. Dozias, J. M. Pouvesle, E. Robert, and C. Pichon, "New Insights on Molecular Internalization and Drug Delivery Following Plasma Jet Exposures," *International Journal of Pharmaceutics* 589 (2020): 119874, https://doi.org/10.1016/j.ijpharm.2020.119874.

38. Y. Ikeda, Y. Hamada, R. Ueshima, et al., "Mechanisms for Introducing 250 Kda Fluorescent Molecules and Cas9/sgRNA into Plant Cells by Plasma Treatment," *Japanese Journal of Applied Physics* 62 (2023): SL1015.

39. K. Tange, T. Hirohata, Y. Ikeda, and M. Jinno, "Helium Atmospheric-Pressure Plasma Jet Enables Macromolecule Introduction in Tomato Stem Sections While Maintaining Short-Term Graft Adhesion," *Plasma Processes and Polymers* 23 (2026): e70128, https://doi.org/10.1002/ppap.70128.

40. R. Zidovetzki and I. Levitan, "Use of Cyclodextrins to Manipulate Plasma Membrane Cholesterol Content: Evidence, Misconceptions and Control Strategies," *Biochimica et Biophysica Acta (BBA) - Biomembranes* 1768 (2007): 1311–1324.

41. B. M. Bigge, N. E. Rosenthal, and P. Avasthi, "Initial Ciliary Assembly Inchlamydomonasrequires Arp2/3 Complex–Dependent Endocytosis," *Molecular Biology of the Cell* 34 (2023): 1–14, https://doi.org/10.1091/mbc.E22-09-0443.

42. B. Labérie, L. Saugé, A. Polesskaya, A. Rousseau, and A. M. Gautreau, "Cold Atmospheric Plasma Promotes Migration Persistence, Through Induced H2O2 and Electric Field," *Biophysical Journal* 125 (2026): 697–708, https://doi.org/10.1016/j.bpj.2025.11.2685.

43. V. Papalazarou and L. M. Machesky, "The Cell Pushes Back: The Arp2/3 Complex is a Key Orchestrator of Cellular Responses to Environmental Forces," *Current Opinion in Cell Biology* 68 (2021): 37–44.

44. Y. Yanagawa, Y. Suenaga, Y. Iijima, A. Okino, and I. Mitsuhara, "Temperature-Controlled Atmospheric-Pressure Plasma Treatment Induces Protein Uptake via Clathrin-Mediated Endocytosis in Tobacco Cells," *Plant Biotechnology* 39 (2022): 179–183, https://doi.org/10.5511/plantbiotechnology.22.0105a.

45. M. Tarek, "Membrane Electroporation: A Molecular Dynamics Simulation," *Biophysical Journal* 88 (2005): 4045–4053.